Soft Matter

Accepted Manuscript

ROYAL SOCIETY OF CHEMISTRY

www.rsc.org/softmatter

Cite this: DOI: 10.1039/c0xx00000x

www.rsc.org/xxxxxx

ARTICLE TYPE

Probe diffusion in phase-separated bicontinuous biopolymer gels

Sophia Wassén,*[a,e] Romain Bordes*[b,e] Tobias Gebäck,[c,e] Diana Bernin,[d,e] Erich Schuster,[a,e] Niklas Lorén,[a,e] and Anne-Marie Hermansson[be]

Received (in XXX, XXX) Xth XXXXXXXXX 20XX, Accepted Xth XXXXXXXXX 20XX

DOI: 10.1039/b000000x

Probe diffusion was determined in phase separated bicontinuous gels prepared by acid-induced gelation of whey protein isolate – gellan gum system. The topological characterization of the phase-separated gel systems is achieved by confocal microscopy and the diffusion measurements are performed using pulsed field gradient (PFG) NMR and fluorescence recovery after photo-bleaching (FRAP). These two techniques gave complementary information about the mass transport at different time- and length scales, PFG NMR provided global diffusion rates in the gel systems, while FRAP enabled the measurements of diffusion in the different phases of the phase-separated gels. The results revealed that the phase-separated gel with the largest characteristic wavelength had the fastest diffusion coefficient, while the gel with smaller microstructures had a slower probe diffusion rate. By using the diffusion data obtained by FRAP and the structural data from confocal microscopy, modelling through lattice-Boltzmann framework was carried out to simulate the global diffusion and verify the validity of the experimental measurements. With this approach it was found that discrepancies between the two experimental techniques can be rationalized in terms of probe distribution between the different phases of the system.

The combination of different techniques allowed the determination of diffusion in a phase-separated biopolymer gel and gave a clearer picture of this complex system. We also illustrate the difficulties that can arise if precautions are not taken to understand the system-probe interactions.

Introduction

Mass transport in soft materials is central for the functionality of many applications. Some illuminating examples can be found in food, hygiene products and pharmaceutical formulations where the performance of the material is largely depending on the control of flow or diffusion properties through its structure at different length scales.[1, 2] Mass transport properties are determined by various mechanisms such as obstruction, friction interactions and interactions of the solute within the matrix and by the structure dynamics.[3-8] In addition, electrostatic interactions, e.g. solutes binding to the gel network, also contribute to modify the transport properties in soft matter.[9-12] Establishing the relationship between the microstructure of the material and flow and diffusion properties remains therefore a challenge, especially in materials with heterogeneous microstructures.[3] It can be addressed by microscopy techniques that allow the determination of characteristic microstructural features of the material[13] combined with the measurements of the diffusion rates of various probes.[14-16] The evaluation of diffusion rate has benefitted from the development of techniques such as pulsed field gradient NMR, [17-19] dynamic light scattering, [20, 21] fluorescence recovery after photobleaching,[14, 22-25] single-particle tracking,[26, 27] fluorescence correlation spectroscopy, [28, 29] raster image correlation spectroscopy[30] which all allow *in-situ* measurements. In most cases, microstructural information in combination with diffusion measurements is applicable for materials that are rather homogeneous at a given length scale. Nevertheless, most of the materials of applicative interest have very complex and heterogeneous microstructures and therefore more research is needed.

Fluorescence recovery after photobleaching (FRAP) and pulsed field gradient (PFG) NMR are commonly used to study mass transport in gel systems and give complementary information about the mass transport at different time- and length scales.[3] NMR provides global diffusion rates in the gel systems, while FRAP enables locally resolved measurements of diffusion in the different phases of the systems. Even though FRAP is often considered as advantageous over NMR in the sense that it allows rapid and spatially resolved measurements, it requires the use of fluorescent probes that may interfere during the diffusion assessment.[12] Addressing these questions by validating the measurements is not trivial but it is crucial to establish a clear picture of the mass transport mechanism in complex systems.

Phase separating systems of gelling biopolymers, commonly found in food, where they serve to control properties like texture and stability,[31, 32] are typical examples of such materials where the resulting morphologies present domains of different natures and with structures ranging over several length scales.[33] Biopolymer mixtures often experience a segregative phase separation through the

mechanism of spinodal decomposition (SD). SD is initially distinguished by the growth of concentration fluctuations within the mixture and the self-similar growth of a characteristic wavelength, which increase when the concentration has reached equilibrium.[34] Gelation of at least one component is common, and has a strong impact on the resulting morphology.[35] By tuning the system properties, gelation rate or composition for instance, the final microstructure of a segregative phase separation can be directed from homogeneous to interconnected bicontinuous morphologies, with domain dimensions ranging from few tenths of nanometers up to hundreds of microns.[33, 36, 37]

In this paper, phase-separated gels of whey protein isolate (WPI) - gellan gum has been investigated with the emphasis on probe diffusion. The bicontinuous microstructures in the gels will be tuned to hold different typical length scales and the structure–diffusion properties will be evaluated by PFG NMR, confocal microscopy, and FRAP. The results obtained will then been compared to the results obtained by Lattice Boltzmann simulations. The objectives were to evaluate the role of the characteristic wavelength, volume fraction, specific surface, tortuosity and equilibrium diffusion probe concentration on the diffusion properties in phase separated gels with self-similar bicontinuous microstructure.

Material and methods

2.1 Materials

Two biopolymers were used in this study: BiPRO™ WPI (kindly provided by Davisco Foods International, Inc., Le Sueur, MI, USA) and Kelcogel© F low acyl gellan gum (obtained from CP Kelco UK Limited, Surrey, UK). d-(+)-gluconic acid δ-lactone (GDL) was purchased from Sigma-Aldrich (St Louis, MO, USA) and FITC-dextran 10 kDa MW, Texas Red sulfonyl chloride and secure-seal spacers from Invitrogen (Eugene, OR, USA).

2.2 Microgel preparation

A stock solution of 9% w/w of WPI BiPRO™ was dissolved in distilled water under stirring for 2 h. WPI aggregates were prepared by incubating the stock solution at 68.5°C for 2.5 h [36, 38] and then cooling down to ambient temperature. A stock solution of 0.6% w/w gellan gum was dissolved in distilled water under stirring for 2 h, and stored at 6°C over night for a complete dehydration. The gellan gum solution was heated to 80°C for 30 minutes, and cooled to ambient temperature prior to use.

The final concentration of the biopolymer mixture used was 3% w/w WPI and 0.04% w/w of gellan gum. For the analysis of the pure gels the WPI aggregate solution was diluted to the required concentration of 3 or 6% w/w of WPI, and the gellan gum to a concentration 0.08% w/w. The gel formation was achieved by a cold-gelation process [36, 38]. d-(+)-Gluconic acid δ-lactone (GDL) was used to induce gelation as it gradually reduces the pH of the solution by a slow hydrolysis of the lactone. Amounts of 0.25% w/w GDL resulted in a decrease of the pH to 4.6 (±0.05) after 48 h incubation at 20°C (±1°C) in bulk phase.

The samples were placed at five different incubation temperatures, 5°C, 8°C, 15°C, 20°C and 35°C (±1°C) respectively, after the mixtures had been stirred carefully for 30 minutes. The same amount of GDL was used in the pure WPI samples and in the mixtures with gellan gum, regardless of the incubation temperature.

Texas Red was used to stain the protein phase fluorescently and allowed visualization in the confocal laser scanning microscope.

The FRAP measurements were done using a 10-kDa FITC-dextran probe in order to study the diffusion coefficient with CLSM. The probe was diluted in pure water before it was added to the sample. The probe concentration was 200 ppm in all samples, chosen to give a linear response in fluorescence versus concentration. A 6-µl aliquot of the biopolymer mixture was added to a secure-seal well, attached on one cover glass, and a second glass was placed on the top.

The samples were analyzed with the confocal microscope 48 h after the gelation process started, to ensure that the final microstructures were obtained. All NMR and FRAP measurements were done at ambient temperature, regardless of incubation temperature, and performed 1 week after the 48 h of incubation.

2.4 Pulsed field gradient NMR measurements

Pulsed field gradient experiments were run on a 14.1 T Bruker spectrometer equipped with a Diff30 probe (maximum gradient strength 12 T m^{-1}) at 20°C. ^{1}H diffusion measurements were carried out in the z-direction by using a standard stimulated echo sequence. The gradient strength, g, was varied between 0.6 and 3 T m^{-1} in 19 steps. The gradient duration δ was set to 1 ms and the time between the leading edges of the two gradient pulses that allow for diffusive motion Δ was set to 100 ms. For each sample, 1032 transients were collected. The processing (phasing, baseline correction and integration) and fitting were done in Matlab (MathWorks, USA). The integrals I of the region between 0.6 – 0.9 ppm methyl groups of alpha-lactalbumin (α-la) (MW ~14,2 kDa, hydrodynamic radius ~ 2 nm of the native protein,[39] IEP 4.2-4.5, α-la does not form gels upon denaturation and acidification) were fit to $I = I_0 \exp(-bD)$ where D is the self-diffusion coefficient, I_0 is the signal intensity at $g = 0$ and the diffusion weighting variable b is given by $\gamma^2 g^2 \delta^2 (\Delta - \delta/3)$ with γ being the magnetogyric ratio. The standard deviation was obtained from 500 Monte-Carlo simulations [39]. The integral range was chosen in order to avoid overlapping with GDL, and no other signals were observed at this range.

2.5 Confocal laser scanning microscope

The confocal laser scanning microscopes (CLSM) utilized in this work was a Leica SP2 AOBS (Heidelberg, Germany). A water objective with a 20-time magnification and a NA of 0.50, was used throughout the study.

2.5.1 Image recording

The light source was an HeNe laser with an emission maximum at 594 nm. The signal emitted in the wavelength interval 605 to 685 nm was recorded. The images were recorded with 1024×1024 pixels and computer zooming of 2×. The CLSM images of the final microstructures were recorded at least 48 h after the samples were prepared.

The fluorescence intensities from the FITC-dextran probe in the two phases were estimated by placing a region of interest (ROI) in the different phases in CLSM images, followed by an intensity area calculation using the Lecia software. Two sets of gels, incubated at 8 and 20°C, were examined. 10 to 15 ROI's in each phase were placed in 10 different images for every gel.

2.5.2 CLSM-FRAP protocol

In the FRAP measurements the light source was an argon laser with 488-nm emission maximum, and the wavelength interval 500 to 600 nm was recorded.

The settings for the FRAP measurements can be found elsewhere.[12] The FRAP protocol consisted of 20 pre-bleach images, one bleach image followed by 50 images on the recovery process. The bleached areas are called region of interest (ROI) and were 30 µm large discs (as standard) at 50-60 µm below the cover glass. In some cases, depending on the size of the microstructure, ROI of 20 µm were used. The requirement of a low NA objective for FRAP restricts the ROI sizes to 10 µm, as for smaller ROI sizes the measurement becomes too noisy; therefore 20 µm were chosen as the smallest ROI to be safe in a regime of a good signal to noise ratio.

The FRAP measurements were done at ambient temperature, regardless of the prior incubation temperature of the gel samples. At least 10 FRAP measurements was performed on different spatial coordinates per sample and/or per region inside a phase-separated sample. Reproducibility was ensured by triplicating samples. During the measurements in one of the regions of a phase-separated structure, the ROI was carefully placed in the region and the microstructure controlled in the z-axis as well to ensure the ROI central positions in the microstructures. In mixtures incubated at 8°C, the measurements were made using ROIs with a diameter of 30 µm. To separate the regions in the somewhat smaller structure of the gels incubated at 15°C a ROI diameter of 20 µm was used. In the measurements to determine the global diffusion rate the ROI was randomly placed in the sample, without consideration of the phase-separated structure.

A pixel-based framework for analysis of FRAP data, developed by Jonasson and co-workers[40] was used to process the data. This model uses a pixel-based statistical methodology of minimizing the likelihood function to solve the diffusion equation and therefore efficiently utilizes all recorded pixel - all the information about the diffusion process - in the available set of image data. The evaluation of the model was carried out in Matlab.

Previous studies have shown that this model is robust and reliable,[24, 41] as long as the initial bleaching profile can be assumed to be approximately Gaussian. The limitations of the model are only reached for slow processes, which exhibit a hat-shaped initial bleaching profile, and when probe-network interactions are not negligible and the diffusion equation does not capture the physics of the system accurately any more.

2.5.3 Evaluation of probe-diffusion influenced by electrostatic interactions

To treat systems in which probe – gel network interactions influence the diffusion behavior, a more detailed framework, FRAP and binding, was needed to analyze the data.

In the FRAP and binding approach the fluorescent recovery of the probes is described by a sum over two states: (a) a free diffusion of the probe in-between binding events and (b) an immobile state in which the probe is 'bound' to the polymer matrix; the crossover between the two states is determined by the corresponding binding pseudo-on and off binding rate constants. Such a framework was developed by Kang and co-workers[42] for FRAP experiments in live cells, and got recently implemented in soft-mater systems to describe the effect of electrostatic interactions upon the probe diffusion of Sodium-Fluorescein in pH 3.5 β-lactoglobulin gels.[12] A more detailed description of the underlying reaction-diffusion equation and the evaluation methodology used is described elsewhere.[12]

This method was used to process the FRAP data and evaluate the binding of the probe to the WPI/gellan gum system at pH 4.6, potentially resulting from electrostatic attractive interactions between negatively charged FITC-dextran and the positive charges of the protein network, allowing for the necessary correction, should the need arise.

2.6 Rheology

Flow sweep measurements of serum from gels incubated at the different temperatures were done using a cone and plate system (40 mm, 0.04 rad) in an ARES G2 rheometer (TA Instruments, New Castle, USA) in order to study the viscosity. The ARES was set to analyze at shear rates 0.1 to 500.0 1/s; 10 points per decade. The measurements were done at 20 °C and all solutions were surrounded with a low viscosity paraffin oil to prevent evaporation. The viscosities reported are the mean values from shear rates between 1-100 1/s.

2.7 Lattice-Boltzmann simulations

2.7.1 Image analysis.

In order to transform the intensities in the 3D image stacks obtained by CLSM to local diffusion coefficients used as input to the diffusion simulations, four steps were performed. First, in order to compensate for the loss of intensity with the depth in the sample, all slices were scaled to have equal average intensity. Then, the data was smoothed using a 3D Gaussian filter with σ=1.5 voxels in order to remove noise which could cause stability problems in the simulations. Upper and lower thresholds were then set for pure WPI and serum phases at 1.5 times the average intensity and 0, respectively. These thresholds corresponded roughly to the peaks in the histogram for high and low intensity. Finally, the intensity data was converted to local diffusion coefficients by setting the diffusion coefficients in the pure WPI phase (at or above upper threshold) and pure serum phase (at lower threshold) to the values obtained from FRAP measurements (see Figure 3) and assuming a linear variation for intermediate intensities.

2.7.2 Lattice Boltzmann simulations

The lattice Boltzmann method is a numerical method for solving partial differential equations, based on the simulation of local particle populations. Here, it was used to solve the diffusion equation with variable equilibrium concentration $c_{eq}(x)$,

$$c_{eq}(x)\frac{\partial X}{\partial t}(x,t) - \nabla \cdot \left(c_{eq}(x)D(x)\nabla \mathrm{X}(x,t)\right) = 0 \qquad (1)$$

with $X(x,t) = c(x,t)/c_{eq}(x)$, for a concentration c of a diffusing species with local diffusion coefficient $D(x)$. $\mathrm{X}(\mathrm{x},\mathrm{t})$ is the molar ratio. One important reason for using the molar ratio is that it is continuous function in all parts of the simulation box and no internal boundary conditions between different regions have to be specified.[43] Thus diffusion across interfaces is naturally implemented in the model. Diffusion along interfaces is not explicitly included in the model. See [43] for a derivation of this equation. Here, c_{eq} assumes different values in the two phases, describing the

equilibrium distribution of the diffusing probe. The space-dependence of c_{eq} was determined using intensity data from the CLSM images just like the local diffusion coefficient $D(x)$, as described in the previous section. Different equilibrium distributions between serum and WPI phase were assumed, ranging from 90% in the serum phase to 10%. The lattice Boltzmann method used here was the two-relaxation-time method with a variable scalar diffusion coefficient, as described in.[44]

The lattice Boltzmann diffusion simulations were performed with the local diffusion coefficient $D(x)$ and equilibrium concentration $c_{eq}(x)$ determined from the CLSM data. To reduce computational time, the data was downsampled to 256x256 voxels in the x-y plane. The total effective diffusion coefficient D_{eff} was measured in the x- and y-directions by applying a relative concentration difference ΔX in this direction and computing the corresponding average diffusive flux j_x (or j_y). D_{eff} was then computed from Fick's law as $D_{\text{eff}} = -j_x L/(\overline{c_{eq}}\Delta X)$, where $\overline{c_{eq}}$ is the volume average of $c_{eq}(x)$. Note that since we divide with $\overline{c_{eq}}$, only relative differences in $c_{eq}(x)$ are important. The average value of D_{eff} between the x- and y-directions was then used for each sample. In the other directions, mirror boundary conditions were used. Diffusion was not simulated in the z-direction since the sample was regarded too thin in this direction to yield correct results. More details on these computations may be found in.[45]

Result and discussion

3.1 Design of the microstructure

The phase-separated gels used in this work consist of a mixture of whey protein isolate (WPI) and gellan gum. The gelation of the system is achieved by an acid-induced gelation,[38, 46] where protein aggregates are first formed in a pre-heating step. The aggregates are prepared at pH that diverges from the protein pI so that the aggregates carry a negative charge and gelation is prevented. The second step involves mixing the WPI-aggregate solution with the polysaccharide, and the addition of an acidifier, d-(+)-Gluconic acid δ-lactone (GDL), which slowly decreases the pH of the solution. As the pH decreases the electrostatic repulsions between the aggregates are reduced and the gelation process starts. Simultaneously, the system undergoes a segregative phase separation that is caused by the molecular immiscibility, initiated as the enthalpy term is reduced when the aggregates starts to form larger clusters (and increase their molecular mass).[33, 37] The segregative phase separation generates two regions, enriched in one polymer and depleted in the other. Here, near-symmetric mixture is used that phase separate through the spinodal decomposition mechanism, and evolves into a bicontinuous microstructure with a self-similar growth of a characteristic wavelength. However, as the pH decreases further the negatively charged polysaccharides starts to interact with the now positively charged protein network. Eventually most gellan gum molecules will be bound on the protein phase,[33, 47] while about 5% of protein fragments usually remains free.[38] The different phases of this system will most likely exhibit considerably different probe diffusion rates, and even though the volume fraction of the gel phase is always about 50% it will give a global diffusion rate that is depending on the microstructure.

Gelation of at least one component will have a strong impact of the final microstructure, as it retards the structure evolution and causes kinetic arrest of the phase separation at a non-equilibrium state. The structure evolution and the final microstructure are determined by the initiation of the phase separation and the gelation, their relative rates as well as the interplay between them. Therefore, by controlling the rate of these processes it is possible to tailor-make the final microstructure of such systems. Extensive research has been done on the structural evolution and final microstructures of numerous phase-separated biopolymer systems that undergo gelation, in both bulk phase and inside confined geometries.[31, 33, 36, 48-53]

The characteristic wavelength of the microstructure of the phase separated WPI-gellan gum systems has been tuned by changing the gelation rate. The polymeric mixtures were incubated at five different temperatures, 5°C, 8°C, 15°C, 25°C and 35°C, respectively. The resulting microstructures are shown in Fig. 1, where it shows that the characteristic wavelength decreases with increasing incubation temperature.

As mentioned, the gelation in this particular biopolymer system is controlled by hydrolysis of the GDL, which rate is temperature dependent. Incubation at the lowest temperature (5 °C, Fig. 1a) resulted in bicontinuous morphology with large interconnected microstructures of a polymer-rich phase (in clear, Fig. 1) and a serum phase (in dark, Fig. 1) i.e. large characteristic wavelength.

Figure 1. CLSM micrographs of phase-separated gels systems composed of 3% w/w WPI and 0.04% w/w gellan gum incubated at different temperatures: 5 °C (a), 8 °C (b), 15 °C (c), 20 °C (d), 35 °C (e).

A low temperature slows down the hydrolysis of GDL and the decrease in pH, which thereby retards the gelation and allows the microstructure to grow larger before the structural evolution is kinetically trapped. Increasing the incubation temperature leads to smaller microstructures, and at the highest incubation temperature (35 °C, Fig. 1e) the gelation rate exceeds the phase separation rate, and the system is restrained to a more homogeneous microstructure with no distinct regions, at the resolution of CLSM. The same composition of the biopolymer mixture, 3% w/w WPI and 0.04% w/w gellan gum was used throughout the study. This allows the study of the mass transport without alteration in the biopolymer concentration, which potentially could have an impact on the diffusion rates.[3]

3.2 Measurements of diffusion properties

In the current set of experiments, the global diffusion has been measured by recording the signal of 10 kDa FITC-dextran and the ^{1}H signal of non-gelled protein fragments, by FRAP and PFG NMR, respectively. PFG NMR provides a global measurement, over a few micrometres in the z-direction, of the diffusion of a probe, intrinsically available in the sample, and this during a diffusion time of around 100 ms. The FRAP techniques give information about the local diffusion properties, typically couple of tens of microns, over a longer time, up to several seconds. Beside the need of a suitable fluorescent probe, FRAP largely differs from NMR in the sense that it enables measurements that are spatially resolved. This has allowed us to determine the diffusion coefficient locally in the different phases of the systems, but also the global mass transport rates in the

phase-separated gels.

3.2.1 Diffusion measurements by PFG NMR

PFG NMR is nowadays routinely used for the measurement of diffusion in homogeneous and heterogeneous materials.[19] In comparison with other techniques to assess mass transport the results will not be biased by the dimensional and time scales. The effect of heterogeneity on a nanometer scale will be averaged thus enabling the measurements of the global diffusion.

The diffusion coefficients in the phase-separated gels systems incubated at 5, 15 and 35°C were determined by recording the decay of the protein signal from fragment of non-gelled α-lactoglobulin (the native protein have a hydrodynamic radius ~2 nm[39]), during standard stimulated spin-echo experiments with varying gradient strength. 5% of the native protein has been found to remain free in solutions of WPI-aggregates.[38, 46] The protein-probe is believed to be homogenously distributed throughout the gel, since serum from WPI-gels mixed with polysaccharides was shown to contain ~0.09% (w/w) of native protein by use of SEC-MALLS (representing 3% of the initiative WPI concentration).[47] Because of a very short relaxation time, the aggregated protein signal contribution was neglected. The measurements were all carried out at 20°C.

Prior to the determination of the diffusion in the phase-separated systems, the mass transport in the pure gel phase was determined i.e. macroscopic WPI gels, as illustrated Fig. 2a. A small decrease can be observed with increasing temperature. The decrease in diffusion rate may arise from differences in the protein network. It was discussed by Alting *et al.*[38] that small amounts of GDL would prolong the time at which the system was situated at the iso-electric point, where the electrostatic interactions are minimal. This was supposed to increase the period of time to form covalent bonds, leading to larger aggregates in the gel. Accordingly, larger aggregates could be created also in our case as the gel incubated at 5°C experience a slower gelation rate. This could result in larger voids in the gel network, since concentration of the protein is equal in all gels, and give rise to the slightly faster diffusion observed in the WPI gel incubated at 5°C.[54]

Figure 2. Pulsed-field gradient NMR diffusion in 3% WPI gels (a) and in phase-separated mixtures of 0.04% gellan gum and 3% WPI (b). All gels were incubated for 48h at the indicated temperature and stored for 1 week at ambient temperature.

Fig. 2b shows the diffusion rates of the protein α-lactalbumin (which is still in solution[47]) in the different phase-separated gels. The results demonstrate a decrease in global diffusion coefficient when the morphology of the system changes from a rather open structure to a structure with smaller domains, i.e. when going from long to short characteristic wavelength.

3.2.2 FRAP measurements

FRAP was used to measure the mass transport of a fluorescent probe, 10-kDa FITC-dextran that has a hydrodynamic radius of about 3.5 nm. The complexity of the microstructure in these bicontinuous gels, but also the interactions between the gel-network and the probe molecules are often at the origin of erroneous measurements. The polymer system used here has a final pH around or lower than the isoelectric point of the protein (IEP β-lactoglobulin pH 5.1), yielding positively charged protein gel-network. The FITC-dextran probe naturally carries a negative charge owing to the presence of the fluorescein. The probe diffusion was in this particular system found to show binding effects during the measurements. In order to take this into account, the FRAP and binding approach was utilized to evaluate binding-corrected values of the diffusion coefficients.[12] Furthermore, binding may influence the probe distribution between the two phases as well.

3.2.2.1 FRAP measurements in phase-separated structures

FRAP measurements were carried out in phase-separated gels. To investigate the global diffusion coefficient the region of interest (ROI) was placed randomly in the gels, without consideration of the position of the ROI in the microstructure. The results are presented in Fig. 3.

Figure 3. The diffusion coefficient for 10-kDa FITC-dextran in phase-separated mixtures of 3% WPI and 0.04% gellan gum, incubated for 48 h at the indicated temperatures and measured after storage for 1 week at ambient temperature. All values have been corrected with regards to electrostatic interactions influencing the diffusion of the probe molecule.

Considering the FRAP measurements in phase-separated gels in Fig. 3, the lowest diffusion coefficients were found for the gels incubated at 20 and 35°C, whereas the highest value was recorded after incubation at 5 °C. These results are in agreement with the trend observed by PFG NMR, however, the absolute values between the NMR and the FRAP cannot be directly compared since the diffusion coefficients are obtained from two different probe molecules. More interestingly, the decrease of the diffusion rate between 5°C and 15°C accounts for 45% when measured by FRAP while the NMR measurements shows a variation of only 17%. Several reasons can explain this large difference. First, it is noteworthy that in the FRAP measurements, the ROI disk has a dimension of the same order as the characteristic dimensions of the structure. This allows FRAP to only give an indicative value of the global mass transport properties. Second, during the measurements, a net attractive interaction was noted between the WPI-network and the probe leading to its depletion in the serum phase. This was noticed by the loss of the fluorescence intensity of the serum phase. The intensity quantification revealed that the quota between the dark and the bright phases was 0.28, giving that almost 4 times as much probe is situated in the WPI-rich phase (equal in both gels evaluated), compared to the serum phase. This value corresponds to a probe concentration of approximately 40 ppm in the serum, which yields a low signal and a noisy recovery curve and an increase in the standard deviations, which are larger than expected.

3.2.2.2 Local diffusion in the different phases obtained by FRAP

As stated earlier, the effective concentrations of the probe in the different phase regions can differ. In addition, in this system the bright phase is composed by both WPI and gellan gum, leading to a different system than the single WPI gel. Therefore, it is essential to measure the local diffusion properties directly in the mixed systems.

FRAP is a suitable technique for analyzing diffusion coefficients in local regions, in the sense that it is spatially resolved and allow the positioning of the ROI either in the bright or in the dark phase. The global measurements in Fig. 4 were made using ROIs that were selected randomly in the samples, without regards if one or two phases were

integrated. By carefully positioning of the ROI in either the brighter biopolymer-rich phase or the darker serum phase, it was possible to measure the diffusion properties in the different regions. The results obtained in gels made at 8 and 15°C are presented in Fig. 4. As expected, the probe diffusion was much faster in the serum phase than in the protein phase for both gels. The global diffusion rate was influenced by both phases, and follows the trend observed in previous measurements, i.e. it was significantly faster in the gels held at 8°C than in those incubated at 15°C. Here the diffusion was measured in a slightly different way than above since only the first 5 post-bleach images (corresponding to a measurement time of 2.5 s) were taken into account, since for this short recovery times the influence of the FITC-dextran in the second phase, in which the ROI was not placed, upon the recovery curve is minor. This explains the discrepancy between the values in Fig. 3 and Fig. 4, even though the trend remains similar regarding the effect of the microstructure.

Figure 4. Diffusion coefficients of the probe 10-kDa FITC-dextran in a phase-separated gel of 0.04% gellan gum and 3% WPI incubated for 48 h at 8 °C (a), and 15 °C (b) after which they were stored at ambient temperature for 1 week. The data was based on the first 5 post-bleach images.

However, it is noteworthy here that the errors significantly increase for the measurements of the serum phase and for the global diffusion, which is believed to be caused by the inhomogeneous distribution and depletion of the probe. In addition, note that also the third dimension of the bicontinuous microstructure can influence the FRAP measurements since a cylindrical region is bleached and the net diffusion in the z-direction is assumed to be minor in the FRAP data evaluation model.[3, 55] To increase the accuracy of the measurements of the probe diffusion the serum was expelled from the phase separated gel 48 h after the mixing point, and then stained by the FITC-dextran probe. The diffusion in the serum phase was found to have a high value, similar to the free diffusion of the FITC-dextran in water (pH 4.6). This indicates that the serum phase has a very low concentration of biopolymers, which also supports the discussion by van der Berg et al..[33, 47] that gellan gum is attracted to the protein phase in the course of gelation.

We carried out similar measurements on serum collected from the gels incubated at different temperature. The results listed in Table 1 shows that the values of self-diffusion in the serum remain invariant of the incubation temperature. The FRAP measurements in the serum show a high coefficient in the range of free diffusion in water for the 10kDa FITC-dextran probe, for all incubation temperatures. The same trend was reflected with rheological measurements (results not shown), where the viscosities of the serums from the different gels had indifferent values, in the magnitude of water. This indicates that the disparity between the diffusion rates found is not caused by differences in viscosity of the serum phase. However, we found that the viscosities of all serums were significantly higher than the viscosity of water (1 mPa•s), indicating that still some polymers remains in the serum phase.

Table 1. Diffusion coefficient of the serum phase from gels prepared at different incubation temperatures, measurements done by FRAP.

Sample	Mass transport ($\mu m^2/s$)
Serum 5°C	70.59 ± 2.87
Serum 8°C	70.81 ± 2.07
Serum 15°C	66.56 ± 3.04
Serum 20°C	67.45 ± 4.54
Serum 35°C	69.11 ± 3.28
Water (pH 4.6)	67,63 ± 3.16

From this series of local measurements, it can be stated that the probe depletion from the serum phases influences the measurements of the local diffusion properties, and that in such case, the collection of the serum from the gel for further measurements enables a less probe depending quantification of the diffusion. Note that the measurements in the bright phase are less affected. This major difference is reflected in the global measurements leading to uncertain absolute value of the diffusion.

3.3 Lattice-Boltzmann simulations

Lattice-Boltzmann simulations have been conducted to evaluate the two experimental methods *in silico*. Additionally, we were able to verify our hypothesis according to which the larger differences observed between the diffusion coefficients determined at different incubation temperatures by FRAP compared to PFG NMR are mainly due to the probe inhomogeneous distribution between the dark and the bright phases. Finally, the diffusion relationship between true diffusion coefficient and microstructure could be established.

Figure 5. Simulated diffusion in bulk phase structures of a mixture of 0.04% gellan gum and 3% WPI incubated at 8 °C (a) and 20 °C (b). The structures are shown at the same scale. The orange parts are the WPI phase. The blue lines are flux lines following the diffusive flux field (computed with an even equilibrium distribution in the two phases) starting from a straight line at the bottom left end of the simulation box.

The first set of simulations was conducted by using the local diffusion values (see section 3.2.2.2) as input for the two phases together with the 3D data of the structure of the bicontinuous microstructure. Diffusion across the interface is implicitly accounted for in the model.[43] Fig. 5 shows the three-dimensional bicontinuous microstructures of 0.04% gellan and 3% WPI incubated at 8 and 20°C. It can be seen that the microstructure is isotropic. In addition, the characteristic wavelengths are present in all three dimensions. Fig. 5 also display the simulated diffusion paths obtained (with equal equilibrium distribution of the probe in the two phases) seen as blue lines protruding the microstructure. In that way, the global effective diffusion coefficients were computed from *x–y* stacks of CLSM images of the microstructured gels, using local effective diffusion coefficients for WPI-rich and serum phases determined locally by FRAP. The simulations were carried out based on the CLSM images obtained at 8°C and 20°C. Above 20°C the CLSM could not resolve the structure well enough to provide input data of acceptable quality to enable a proper simulation, as can be seen from Fig. 1e. The results from this first set of simulations, assuming an equal distribution of the probe in the bright and the dark phase, showed that there was no difference between the gels

incubated at different temperatures, which was contradictory to the overall tendency observed by PFG NMR and FRAP.

Therefore, further simulations were conducted using the same CLSM data, but using the values of diffusion coefficients measured after the addition of 10 kDa FITC-dextran to the expelled serum phase (see Table 1) while the diffusion coefficient in the WPI phase was taken as the value of the local measurements as before. The average values of the measured diffusion coefficients were used as input to the simulations for both 8°C and 20°C samples. Furthermore, a range of different equilibrium distributions of the probe between the two phases was assumed and used in equation (1). Five different distributions were used, ranging from 10% of the probe in the WPI phase to 90% in the WPI phase.

Fig. 6 and Table 2 summarize the results obtained from the diffusion simulations through the bulk structures and the results from the image analysis, i.e. volume fraction and specific surface. In addition to the effective diffusion coefficients, the simulations have allowed the calculation of the tortuosity, from the average length of the flux lines, taking into account the different local effective diffusion coefficients.

3.3.1 Effective diffusion constants

From the computed effective diffusion constants in Fig. 6, it is clear that the global diffusion becomes slower when more of the probe is located in the WPI-rich phase, which is natural since diffusion in this phase is slower. Furthermore, with more probe in the WPI phase, the relative difference between the 8°C and 20°C samples becomes more pronounced, with about 12% slower diffusion in the gel incubated at 20°C with 75% and 90% of the probe in the WPI phase (the equilibrium concentration of probe in the WPI-rich phase was estimated to approximately 78%, see section 3.2.2.2). Both the absolute numbers of the effective diffusion coefficient and the difference between samples agree as well as can be expected with the FRAP data in Fig. 4, where the difference between the 8°C and 15°C samples is about 23%.

Figure 6. Simulated effective diffusion coefficients with varying probe equilibrium distribution between the two phases for gels incubated at 8 °C and 20 °C (top) and relative difference between the effective diffusion coefficients at 20 °C compared to at 8 °C for the different probe equilibrium distributions (bottom). The error bars show standard deviations over the samples.

Table 2. Data on the structures at 8 and 20°C, obtained from diffusion simulations and analysis of CLSM image stack data. The volume fraction of serum was computed assuming a sharp division of the two phases at image intensity midway between the two pure phases, and the specific surface was computed using the area of the isosurface at this level. The local effective diffusion coefficients used as input to the simulations were computed from the measurements done by FRAP, and are listed in the two last rows. (* average of measurements done on expelled serum, ** measurements done in situ)

	8°C (N=5)	20°C (N=7)	Change
Tortuosity from eq. (3) (50% in WPI phase)	1.401 ± 0.032	1.379 ± 0.029	-1.6%
Tortuosity from paths (50% in WPI phase)	1.102 ± 0.011	1.086 ± 0.010	-1.5%
Volume fraction serum	0.477 ± 0.017	0.422 ± 0.023	-11.5%
Specific surface (μm^{-1})	0.050 ± 0.002	0.105 ± 0.006	110%
D_{serum} ($\mu m^2/s$)	68.90*	68.90*	-
D_{WPI} ($\mu m^2/s$)	2.463**	2.463**	-

3.3.2 Geometric properties

The computations done on the CLSM stacks show a larger specific surface for the phase interface in the 20°C samples compared to the 8°C samples owing to the fact that the phase separation is less progressed and that the characteristic wavelength is on a finer scale at higher temperature, which is also evident from Fig. 5 and Fig. 1. The increase of specific surface is correlated with decreasing overall diffusion coefficient. This indicates that the amount interface and the diffusion properties and the probe equilibrium concentration in the interface can influence the overall diffusion coefficient. Furthermore, the serum volume fractions are rather close to 0.5 for both incubation temperatures, but with a slightly higher value for the sample incubated at 8°C. Note that the fact that the volume fractions computed in this way differ does not mean that the amount of WPI in the samples differ, but rather reflects the differences in distribution and internal structure of WPI, presumably with a higher density of the WPI phase in the 8°C case. Potentially, this could be cause by the gellan gum as well, which has been found to undergo a coil-to-helix transition at lower temperature and it was argued to influence the phase separation rate.[37] The transition of the polysaccharide was discussed to result in an extended phase separation due to increased charge density and thereby more incompatibility between the gellan gum and the WPI aggregates. This could in turn affect the volume fraction in the phase-separated system and the density of the phases.

3.3.3 Tortuosity estimates

In order to study the reason for the differences in effective diffusion coefficients in a material, an empirical formula is often used (see e.g.[56]):

$$D_{\text{eff}} = D_0 \frac{\varphi}{\tau^2} \qquad (2)$$

where φ is the porosity, D_0 the free diffusion coefficient and τ the tortuosity. It should be noted that the tortuosity here is not necessarily the tortuosity of actual paths through the structure (defined as $\tau = L'/L$, where L' is the length of the path and L is the thickness of the sample), but rather a constant including geometrical effects on the diffusion, apart from the volume fraction. It is easily seen from equation (2) that D_{eff} is scale-independent, since both volume fraction and tortuosity are dimensionless, meaning that just rescaling the structure does not change the effective diffusion constant. Although this may seem counter-intuitive, it is true in general, irrespective of the accuracy of equation (2), and means that the difference in D_{eff} between samples incubated at different temperatures cannot be attributed to the differences in size of the microstructure if the structure is self-similar (as seen in Fig. 5).

First the tortuosity was computed from the average length of randomly sampled flux lines (blue lines, Fig. 6), with the results shown in Table 2. By doing this, the real diffusion coefficient of the WPI phase is considered and the tortuosity reflects the tendency of molecules to take a longer path to avoid the phase that is more difficult to penetrate. In other words, the tortuosity takes into account the effect of both

phases in terms of diffusion and volume fraction and is related to actual paths through the structure. The tortuosity calculated in this way also shows slightly higher values in the 8°C samples (i.e. paths are longer). The flux lines in Fig. 6 also appear to be straighter in the 20°C case, passing through small regions of WPI phase. Thus the change in overall diffusion properties between 8°C and 20°C can't be explained the tortuosity computed from the average length of randomly sampled flux lines in accordance with equation (2).

Equation (2) is generally applied to a situation where one phase is completely impermeable to the solute, which is not the case here. Therefore, we use a corresponding, more general, equation (derived in Appendix A) which includes two phases and an equilibrium distribution of the probe, namely:

$$D_{\text{eff}} = \frac{\varphi_s\, c_{eq}^{(s)}\, D_s + \varphi_w\, c_{eq}^{(w)}\, D_w}{\varphi_s\, c_{eq}^{(s)} + \varphi_w\, c_{eq}^{(w)}}\, \frac{1}{\tau^2}\,, \qquad (3)$$

where *s* and *w* refer to the serum and WPI phase, respectively. Note that since the c_{eq} appears both in numerator and denominator, it is again only necessary to know the relative probe equilibrium concentration in the two phases. Note also that the large difference in diffusion coefficient between the two phases ($D_s/D_w \approx 28$) means that the serum term dominates the numerator in equation (3) for all the different equilibrium distributions used here.

The results from computing the tortuosity using equation (3) are shown in Table 2. The difference in tortuosity between the two incubation temperatures is very small, indicating that the difference in effective diffusion coefficient is mainly due to different volume fractions or the amount and properties of the interface. However, the large tortuosity values around 1.4 indicate that there is a significant effect on the diffusion in the gels not ascribable to the volume fraction, and that equation (3) cannot be used directly to compute D_{eff} when τ is unknown. This effect is not dependent on the incubation temperature, but it does depend on c_{eq} (data not shown), varying from about 1.55 at 10% in the WPI phase to 1.2 at 90% in the WPI phase. This may be explained by that there is not a single tortuosity for the sample, but rather that it depends on the paths molecules take through the sample, which in turn depend on the equilibrium distribution of the probe.

This illustrates that the tortuosity in equations (2) and (3) is not the pure tortuosity of the structure, but rather a factor including all unknown effects not accounted for. In contrast, the detailed picture received through simulations allows us to separate different effects, though at the loss of the (apparent) simplicity of equation (3).

Conclusions

The determination of the mechanism of mass transport properties in phase separated system is a complex task that requires a more elaborated arsenal of techniques than for homogenous gels. In the present work PFG NMR and FRAP have been combined to determine the global and local diffusion rates in model systems made of WPI and gellan gum in which the microstructure can be tuned, in term of scale, by controlling the rate of gelation and thus the segregative phase separation process. The global diffusion measurements in phase separated gels with bicontinuous microstructures showed that the samples with longer characteristic wavelength, those incubated at a lower temperature, had a higher mass transport rate. Probe diffusion measurements using PFG NMR and FRAP showed similar trends, but the relative values differed. The local measurements of diffusion carried out by FRAP in WPI-rich and serum phases showed that depletion of the fluorescent probe from the serum phase influenced the FRAP measurements and care has to be taken with regard to the probe distribution, size of the bleaching region and location of the FRAP measurements.

The microstructures of the phase separated gels were imaged by CLSM and the produced 3D data were used for the simulation with the lattice-Boltzmann method. The modeling allowed the evaluation of the quality of the measurements by relating the global diffusion to the local measurements. It showed that the distribution of the probe was at the origin of the discrepancy between NMR and FRAP in the general trend observed. In addition, the simulation revealed that the differences in diffusion properties between the phase separated gels with different characteristic wavelength depend on the volume fraction. It also appeared that the specific surface for the phase interface can influence the overall diffusion rate. Furthermore, the simulations displayed that the tortuosity computed from the average length of randomly sampled flux lines cannot explain the effect of the characteristic wavelength on the diffusion. A modified tortuosity equation that takes the effect of probe equilibrium concentration into account was used. This enabled further analysis of the simulation data and the computation of tortuosity by the use of the diffusion paths. The tortuosity revealed, because of the partial permeability of the protein-rich phase, the importance of the role of the microstructure in the mass transport properties and that a fine control of such morphology is of highest importance for the design of material with well-defined properties.

Acknowledgements

The collaborations and financial support from SuMo Biomaterial is highly appreciated from all authors. The Swedish NMR Centre is acknowledged for spectrometer time.

Notes

[a] *Structure and Material Design, SIK – The Swedish Institute for Food and Biotechnology, P.O. Box 5401, 402 29 Gothenburg, Sweden. E-mail: sophia.wassen@sik.se; Tel: +46105166609*
[b] *Department of Chemical and Biological Engineering, Chalmers University of Technology, 412 96 Gothenburg, Sweden. E-mail: bordes@chalmers.se; Tel: +46317722976*
[c] *Department of Mathematical Science, Chalmers University of Technology and University of Gothenburg, 412 96 Gothenburg, Sweden .*
[d] *Swedish NMR Centre, University of Gothenburg, 405 30 Gothenburg, Sweden .*
[e] *Vinn Excellence Center SuMo Biomaterials, Chalmers University of Technology and University of Gothenburg, 412 96 Gothenburg, Sweden*

References

1. M. Nydén, N. Lorén and A.-M. Hermansson, in *Water Properties of Food, Pharmaceutical, and Biological Materials*, eds. M. d. P. Buera, J. Welti-Chanes, P. J. Lillford and H. R. Corti, CRC Press, 2006, pp. 79-100.

2. N. A. Peppas, P. Bures, W. Leobandung and H. Ichikawa, *European Journal of Pharmaceutics and Biopharmaceutics*, 2000, **50**, 27-46.
3. N. Lorén, M. Nydén and A.-M. Hermansson, *Advances in Colloid and Interface Science*, 2009, **150**, 5-15.
4. B. Amsden, *Macromolecules*, 1998, **31**, 8382-8395.
5. L. Masaro and X. X. Zhu, *Progress in Polymer Science*, 1999, **24**, 731-775.
6. B. Amsden, *Macromolecules*, 1999, **32**, 874-879.
7. L. Johansson, C. Elvingson and J. E. Loefroth, *Macromolecules*, 1991, **24**, 6024-6029.
8. R. J. Phillips, W. M. Deen and J. F. Brady, *AIChE Journal*, 1989, **35**, 1761-1769.
9. E. M. Johnson, D. A. Berk, R. K. Jain and W. M. Deen, *Biophysical Journal*, 1995, **68**, 1561-1568.
10. N. Hirota, Y. Kumaki, T. Narita, J. P. Gong and Y. Osada, *The Journal of Physical Chemistry B*, 2000, **104**, 9898-9903.
11. N. Fatin-Rouge, A. Milon, J. Buffle, R. R. Goulet and A. Tessier, *Journal of Physical Chemistry B*, 2003, **107**, 12126-12137.
12. E. Schuster, A.-M. Hermansson, C. Ohgren, M. Rudemo and N. Lorén, *Biophysical Journal*, 2014, **106**, 253-262.
13. B. Walther, N. Lorén, M. Nydén and A.-M. Hermansson, *Langmuir*, 2006, **22**, 8221-8228.
14. Y. Cheng, R. K. Prud'homme and J. L. Thomas, *Macromolecules*, 2002, **35**, 8111-8121.
15. A. Pluen, P. A. Netti, R. K. Jain and D. A. Berk, *Biophysical Journal*, 1999, **77**, 542-552.
16. J. Hagman, Chalmers University of Technology, 2012.
17. W. S. Price, *Concepts in Magnetic Resonance*, 1997, **9**, 299-336.
18. J. R. Singer, *Journal of Physics E: Scientific Instruments*, 1978, **11**, 281.
19. D. Bernin and D. Topgaard, *Current Opinion in Colloid & Interface Science*, 2013, **18**, 166-172.
20. W. Brown, *Dynamic light scattering: the method and some applications.* , Clarendon Press, Oxford, 1993.
21. B. J. Berne and R. Pecora, *Dynamic light scattering: with applications to chemistry, biology, and physics* Courier Dover Publications, 2000.
22. J. Hagman, N. Lorén and A.-M. Hermansson, *Food Hydrocolloids*, 2012, **29**, 106-115.
23. H. Deschout, J. Hagman, S. Fransson, J. Jonasson, M. Rudemo, N. Lorén and K. Braeckmans, *Optics Express*, 2010, **18**, 22886-22905.
24. J. Hagman, N. Lorén and A.-M. Hermansson, *Biomacromolecules*, 2010, **11**, 3359-3366.
25. N. Lorén, J. Hagman, J. K. Jonasson, H. Deschout, D. Bernin, F. Cella, A. Diaspro, J. McNally, M. Amelott, N. Smisdom, M. Nydén, A.-M. Hermansson, M. Rudemo and K. Braeckmans, *Submitted*, 2014.
26. V. Levi, Q. Ruan and E. Gratton, *Biophysical Journal*, 2005, **88**, 2919-2928.
27. M. J. Saxton, *Biophysical Journal*, 1997, **72**, 1744-1753.
28. K. Oleg and B. Grégoire, *Reports on Progress in Physics*, 2002, **65**, 251.
29. S. T. Hess, S. Huang, A. A. Heikal and W. W. Webb, *Biochemistry*, 2001, **41**, 697-705.
30. M. A. Digman, P. Sengupta, P. W. Wiseman, C. M. Brown, A. R. Horwitz and E. Gratton, *Biophysical Journal*, 2005, **88**, 33-36.
31. I. T. Norton and W. J. Frith, *Food Hydrocolloids*, 2001, **15**, 543-553.
32. S. Kasapis, *Critical Reviews in Food Science and Nutrition*, 2008, **48**, 341-359.
33. L. van den Berg, Y. Rosenberg, M. A. J. S. van Boekel, M. Rosenberg and F. van de Velde, *Food Hydrocolloids*, 2009, **23**, 1288-1298.
34. J. W. Cahn, *Journal of Chemical Physics*, 1965, **42**, 93-99.
35. N. Lorén, A. Altskär and A.-M. Hermansson, *Macromolecules*, 2001, **34**, 8117-8128.
36. S. de Jong and F. van de Velde, *Food Hydrocolloids*, 2007, **21**, 1172-1187.
37. S. de Jong, H. J. Klok and F. van de Velde, *Food Hydrocolloids*, 2009, **23**, 755-764.
38. A. C. Alting, R. J. Hamer, C. G. de Kruif and R. W. Visschers, *Journal of Agricultural and Food Chemistry*, 2000, **48**, 5001-5007.
39. J. S. Alper and R. I. Gelb, *Journal of Physical Chemistry*, 1990, **94**, 4747-4751.
40. J. K. Jonasson, N. Lorén, P. Olofsson, M. Nydén and M. Rudemo, *Journal of Microscopy*, 2008, **232**, 260-269.
41. J. K. Jonasson, J. Hagman, N. Lorén, D. Bernin, M. Nydén and M. Rudemo, *Journal of Microscopy*, 2010, **239**, 142-153.
42. M. Kang, C. A. Day, E. DiBenedetto and A. K. Kenworthy, *Biophysical Journal*, 2010, **99**, 2737-2747.
43. H. Hagslätt, B. Jönsson, M. Nydén and O. Söderman, *Journal of Magnetic Resonance*, 2003, **161**, 138-147.
44. I. Ginzburg, *Advances in Water Resources*, 2005, **28**, 1171-1195.
45. T. Geback and A. Heintz, *Communication in Computationnal Physics*, 2014, **15**, 487-505.
46. A. C. Alting, R. J. Hamer, C. G. de Kruif, M. Paques and R. W. Visschers, *Food Hydrocolloids*, 2003, **17**, 469-479.
47. L. van den Berg, T. van Vliet, E. van der Linden, M. A. J. S. van Boekel and F. van de Velde, *Food Hydrocolloids*, 2007, **21**, 420-432.
48. S. Wassén, N. Loren, K. van Bemmel, E. Schuster, E. Rondeau and A.-M. Hermansson, *Soft Matter*, 2013, **9**, 2738-2749.
49. S. Wassén, E. Rondeau, K. Sott, N. Lorén, P. Fischer and A.-M. Hermansson, *Food Hydrocolloids*, 2012, **28**, 20-27.
50. S. Fransson, N. LoreÌ n, A. AltskaÌ`r and A.-M. Hermansson, *Biomacromolecules*, 2009, **10**, 1446-1453.
51. H. Firoozmand, B. S. Murray and E. Dickinson, *Food Hydrocolloids*, 2012, **26**, 286-292.
52. M. F. Butler and M. Heppenstall-Butler, *Food Hydrocolloids*, 2003, **17**, 815-830.
53. N. Lorén and A.-M. Hermansson, *International Journal of Biological Macromolecules*, 2000, **27**, 249-262.
54. B. Walter, N. Lorén, M. Nydén and A.-M. Hermansson, *Langmuir*, 2006, **22**, 8221-8228.
55. I. F. Sbalzarini, A. Mezzacasa, A. Helenius and P. Koumoutsakos, *Biophysical Journal*, 2005, **89**, 1482-1492.
56. L. Shen and Z. Chen, *Chem. Eng. Sci.*, 2007, **62**, 3748-3755.

Appendix A. Derivation of equation (3)

In this appendix, we derive equation (3) from considerations similar to the ones leading to the more common equation (2). We consider a system consisting of two phases, with effective diffusion coefficients D1 and D2, respectively. We assume now the very special case that the phases form two parallel channels in the direction of the concentration gradient over the material, so that the cross-sectional area of each phase is constant (though the shape of the cross-section is irrelevant). The volume fractions (and cross-sectional area fractions) are denoted phi1 and phi2=1-phi1, respectively.

In order to compute the effective diffusion coefficient of this system, we apply a difference in the quantity $X = c/c_{eq}$ (see equation (1)) across the x-direction, say, of the material, namely $\Delta X = X_{out} - X_{in}$. The steady-state solution to the diffusion equation (1) is then one where the flux $\vec{j} = -c_{eq}\, D\, \nabla X$ is constant and completely in the direction of the gradient and there is no net flux between the phases. The total flux through the sample is then

$$j_{\text{tot}} = j^{(1)}\,\varphi_1 + j^{(2)}\varphi_2 = -\left(c_{eq}^{(1)} D_1 \varphi_1 + c_{eq}^{(2)} D_2 \varphi_2\right)\frac{\Delta X}{L},$$

where L is the thickness of the sample in the x-direction.

From this, as described in section 2.7, we see that the effective diffusion coefficient is

$$D_{\text{eff}} = -\frac{j_{\text{tot}}}{\overline{c_{eq}}\,\frac{\Delta X}{L}} = \frac{c_{eq}^{(1)} D_1 \varphi_1 + c_{eq}^{(2)} D_2 \varphi_2}{c_{eq}^{(1)} \varphi_1 + c_{eq}^{(2)} \varphi_2}.$$

In case the phases do not form parallel channels, as is usually the case, we add a tortuosity factor $1/\tau^2$, by analogy with equation (2), to account for the tortuous paths through the structure. This yields equation (3). The tortuosity factor is of course a gross over-simplification, but serves its purpose here just as in equation (2) for porous systems.

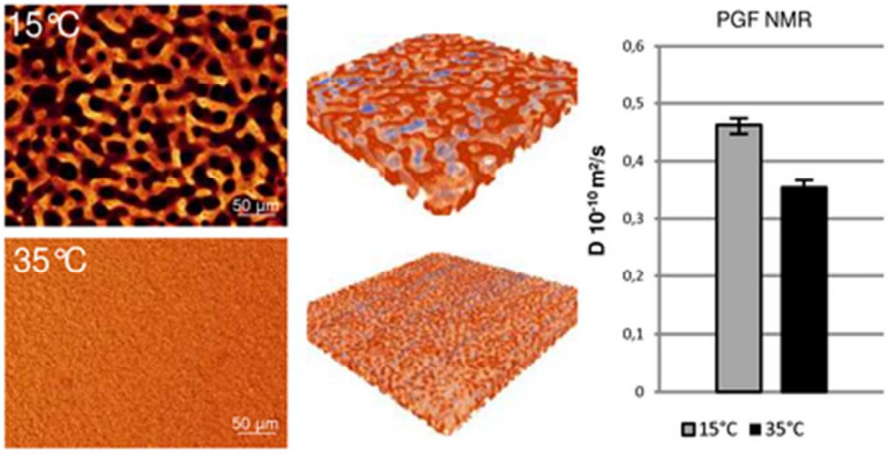

The diffusion in a phase-separated biopolymer gel system is experimentally investigated by FRAP, and PFG-NMR and compared with lattice-Boltzmann simulations.
39x19mm (300 x 300 DPI)